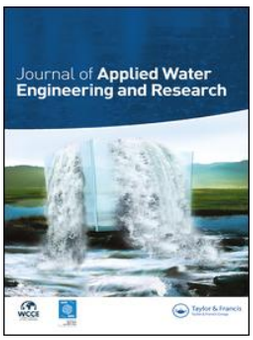

Journal of Applied Water Engineering and Research

ISSN: (Print) 2324-9676 (Online) Journal homepage: https://www.tandfonline.com/loi/tjaw20

Field and model tests of riprap on steep slopes exposed to overtopping

Priska H. Hiller, Leif Lia & Jochen Aberle

To cite this article: Priska H. Hiller, Leif Lia & Jochen Aberle (2019) Field and model tests of riprap on steep slopes exposed to overtopping, Journal of Applied Water Engineering and Research, 7:2, 103-117, DOI: 10.1080/23249676.2018.1449675

To link to this article: https://doi.org/10.1080/23249676.2018.1449675

Journal of Applied Water Engineering and Research, 2019
Vol. 7, No. 2, 103–117, https://doi.org/10.1080/23249676.2018.1449675

Field and model tests of riprap on steep slopes exposed to overtopping

Priska H. Hiller [a,b*], Leif Lia [a] and Jochen Aberle [a,c]

[a] *Department of Civil and Environmental Engineering, NTNU Norwegian University of Science and Technology, Trondheim, Norway;* [b] *The Norwegian Water Resources and Energy Directorate, Central Region, Trondheim, Norway;* [c] *Leichtweiß-Institute for Hydraulic Engineering and Water Resources, Technische Universität Braunschweig, Braunschweig, Germany*

(*Received 27 January 2017; accepted 1 December 2017*)

The comparability of large-scale field tests of dumped and placed riprap with a stone diameter of 0.37 m and corresponding model tests in a scale of 1:6.5 was investigated in terms of stability, packing density and visually observed flow pattern. The tested riprap protections were exposed to overtopping on a slope of 1:1.5 (vertical: horizontal). The results for dumped riprap revealed similarity between the field and model tests based on the critical stone-related Froude number as a measure of the stability, packing density, flow pattern and overtopping depth. The field and model tests with placed riprap showed good agreement in regard to flow pattern and overtopping depth. However, the placed riprap in the model tests was denser packed and more stable than in the field indicating laboratory effects. Placed riprap withstood up to 10 times higher unit discharges than dumped riprap, 6–8 $m^2 s^{-1}$ in the field tests.

Keywords: field and model tests; overtopping; riprap; steep slope;

1. Introduction

Riprap consisting of large natural rocks or artificial elements is widely used to protect river banks, streambeds, bridge piers and abutments, dams, shorelines and other hydraulic structures against the impact of currents and waves (e.g. Abt and Johnson 1991; CIRIA et al. 2007; Abt et al. 2013; Chanson 2015; Jafarnejad et al. 2016). There exist two general riprap types, dumped and placed, which are constructed by either dumping the riprap elements or placing them in an interlocking pattern. The construction of placed riprap is more cost- and labour-intensive than simply dumping elements (Peirson et al. 2008), but placed riprap can withstand higher discharges than dumped riprap constructed with the same stone size (Larsen et al. 1986; Peirson et al. 2008; Hiller et al. 2017), especially on steep slopes (Dornack 2001).

An application of placed riprap within dam engineering is to protect the downstream slopes of embankment dams against erosion due to accidental leakage or overtopping (Toledo et al. 2015). Embankment dams fail statistically more often than concrete dams, and the most common cause for dam failure is overtopping (ICOLD 1995). Overtopping is mainly associated with the inadequate design of spillways (Harris 2015), and enhancing the resistance of embankment dams against erosion from overtopping will thus increase their safety. Additionally, a specifically lowered part on small embankment dams (dam height lower than 10 m), secured with placed riprap, can be an alternative and cost-effective spillway solution (e.g. Larsen et al. 1986; Dornack 2001; Siebel 2007).

In order to increase the resistance against erosion from accidental leakage and overtopping, the downstream slopes of rockfill dams in Norway are secured by a single layer of placed riprap. For this purpose, the riprap stones are placed in an interlocking pattern with their longest axes inclined towards the dam, as shown in Figure 1 and prescribed by OED (2009). The typical downstream slope of embankment dams in Norway is 1:1.5 (vertical: horizontal), corresponding to a slope of $S = 0.67$, and the recommended stone size for the placed riprap is in the range of 0.3–0.7 m, dependent on the consequences in case of dam failure (NVE 2012). In the near future, many Norwegian dams need to be upgraded because they were constructed in the period of 1960–1990, and periodical reassessments often reveal that they do no longer comply with the current dam safety regulation (OED 2009), which applies retroactively. If required, the upgrade includes a new construction or rebuilding of placed riprap on the downstream slope of dams. This aspect has triggered the present research project with the aim to evaluate existing stability approaches of placed riprap on steep slopes and to optimise the design of placed riprap.

Almost all available approaches for the sizing of riprap stones exposed to an overtopping flow have been developed on the basis of physical model tests. However, most of the corresponding studies focused on milder slopes, and data for steep slopes of up to $S = 0.67$ are rare. In addition, most tests were executed with riprap stones smaller than 0.1 m, and data from experiments with large stones are

*Corresponding author. Email: priskahe@alumni.ntnu.no

Figure 1. Rehabilitation work on the 129 m high dam Svartevatn in Norway. The riprap stones on the downstream slope are placed one by one in an interlocking pattern with their longest axes inclined towards the dam. The inclination angle β is the angle between the longest axis of a stone and the slope as indicated in the picture. (Photo NTNU).

desirable for the validation of existing design approaches (Peirson and Cameron 2006; Abt et al. 2013). Furthermore, a comparison between prototype and laboratory tests can provide information to what extent construction-related properties of placed riprap such as placement density and internal friction affect riprap stability. Those properties may moreover be prone to laboratory effects (Pardo et al. 2014).

Facilities offering the possibility to carry out prototype-scale riprap tests are rare due to the required boundary conditions (e.g. steep slopes, dam height, discharge, stone size) and are normally located outdoors (e.g. at the Engineering Research Center of the Colorado State University in Fort Collins). In the framework of the present study, a temporary site became available in Norway, and the opportunity was used to conduct riprap stability test with large stones in order to address the aforementioned challenges.

The objective of the present paper is to investigate the comparability of stability tests with placed riprap at large-scale and equivalent model tests at a smaller scale. Results from additional tests with dumped riprap at both scales will be used to consider the stability gain by placing riprap stones in an interlocking pattern, and to facilitate cross-comparison of the results with outcomes from existing studies. Note that in the present study, the riprap structures were solely exposed to overtopping (i.e. the current was parallel to the slope).

2. Background

2.1. Riprap parameters

The parameters affecting riprap stability can be subdivided into geotechnical riprap properties, properties of the overtopping flow and geometric boundary conditions. Riprap properties are typically characterised by the stone size d, stone density ρ_s, the grain size distribution and the riprap layer thickness. Construction-related properties such as packing densities (i.e. number of stones per unit area) are used to describe the quality of the placement. The dimensionless packing factor P_c defined by Linford and Saunders (1967) and Olivier (1967)

$$P_c = \frac{1}{N d_s^2} \tag{1}$$

relates the number of stones per m^2, N, to the squared stone size of the equivalent stone diameter d_s (diameter of a sphere having the same volume as an average riprap stone). The packing factor P_c is scale-independent, and typical values range from 0.8 (stones placed on edge) to 1.2 (dumped stones); P_c is smaller for a densely packed riprap compared to a dumped riprap. Dependent on the shape and arrangement of the riprap stones, low packing factors can be achieved, for example, $P_c \approx 0.4$ when placing oblong stones with a ratio of $a/b_s = 2.0$ on edge (Linford and Saunders 1967; a denotes the longest axis of the stone and

b_s the average of the intermediate and shortest stone axis b and c, respectively).

The overtopping flow can be characterised by the Froude number $\mathsf{F} = v/(gh)^{0.5}$ where v denotes the flow velocity, g the gravitational acceleration and h the water depth. During overtopping, the flow accelerates from the crest along the downstream slope until the flow is fully developed, meaning that $\mathsf{F} = 1$ at the dam crest and $\mathsf{F} > 1$ further downstream if backwater effects are absent. The flow pattern also depends on the roughness of the riprap, the slope and the discharge. Similar to stepped spillways, it can be characterised by self-aeration and may resemble a skimming flow pattern (Pagliara et al. 2010).

The definition of water depth h (and implicitly of the velocity v) for such conditions is difficult because, on the one hand, aeration hampers the definition of the water surface level (e.g. Bung 2013) and, on the other hand, the associated rough bed conditions require the definition of an arbitrary reference level for the determination of the water depth (e.g. DVWK 1990). Using the discharge per unit width $q = vh$, however, it becomes possible to avoid arbitrary definitions given that the cross-sectional width does not change. Using q, a stone-related Froude number $\mathsf{F}_s = q/(gd^3)^{0.5}$ can be formulated through the combination of the Froude number with the relative submergence h/d. At critical conditions (i.e. riprap failure), F_s becomes

$$\mathsf{F}_{s,c} = \frac{q_c}{\sqrt{gd^3}} \tag{2}$$

where q_c denotes the discharge per unit width at riprap failure. The geometric boundary conditions of riprap are characterised by the slope S, the length L_s covered by the riprap and the width B of the channel or dam. These parameters are of importance for the failure mechanisms as discussed in the following.

2.2. Failure mechanisms

Riprap stability, or failure, needs to be considered in the light of different failure mechanisms for dumped and placed riprap. For dumped riprap, failure is usually considered when the underlying filter layer is exposed to the flow due to the erosion of the riprap (e.g. Linford and Saunders 1967; Abt and Johnson 1991; Robinson et al. 1998; Peirson et al. 2008). If the same definition is applied for a single-layer placed riprap, this would mean that erosion of a single stone would correspond to riprap failure because the filter will be exposed at this particular location. However, if a stone is eroded out of a placed riprap, the remaining stones can absorb the loss because the interlocking pattern allows for the formation of a bearing structure. Therefore, progressive erosion of the riprap layer should be considered as the critical condition (Larsen et al. 1986; Sommer 1997; Dornack 2001; Hiller et al. 2017). Note that dumped and placed riprap may also fail via sliding if the friction forces between the filter and the riprap layer exceed a critical threshold. However, this failure mechanism is not in the scope of the present paper. Similarly, the global stability of the embankment such as safety against overturning or sliding circles, as e.g. summarised in Larsen et al. (1986) or Morán and Toledo (2011), is not discussed in this paper.

The interlocking between the stones in placed riprap allows for, besides the aforementioned bearing structure, the transfer of longitudinal forces. If these forces exceed a critical threshold, the riprap layer can be disrupted (Dornack 2001; Siebel 2007), or displacements of riprap stones can be triggered. The latter can cause failure of placed riprap, as displacements can gradually accumulate and create a gap within the riprap. If a larger gap develops, adjacent riprap stones may lose their interlocking placement and be eroded by the overtopping flow (Larsen et al. 1986; Sommer 1997; Hiller et al. 2017). In general, the largest gap can develop at the transition between the horizontal dam crest and the dam slope. It is worth mentioning that this transitional area has also been identified as a vulnerable area with regard to flow attack in investigations on the breach formation of dams, which were not additionally secured with riprap (e.g. Løvoll 2006; Morris et al. 2007; Schmocker et al. 2013).

2.3. Riprap stability approaches

There exist numerous approaches to estimate the stability of both dumped and placed riprap. A recent summary of design relationships for dumped riprap exposed to overtopping, including data of corresponding stability studies, has been presented by Abt et al. (2013). These data are plotted in Figure 2(a) along with data from Godtland (1989), Larsen et al. (1986), Peirson et al. (2008) and Hiller et al. (2017) showing the critical stone-related Froude number $\mathsf{F}_{s,c}$ as a function of the slope S. The figure also contains the results of the model tests reported by Lia et al. (2013), but the data from their field tests are not included due to the reasons discussed below. In order to visualise the variability of the stone size d used in the corresponding studies, the marker size is proportional to this parameter in Figure 2(a,b). Figure 2(a) illustrates that stability data for dumped riprap with large stone sizes or at steep slopes are rare. In fact, 75% of the data points presented by Abt et al. (2013) were obtained for $S \leq 0.2$, and less than 24% of the data points were obtained in studies with stone diameters $d > 0.1$ m. Moreover, only four of their presented 96 data points were obtained in studies with $d > 0.2$ m (extracted from Mishra 1998 and Robinson et al. 1998) even though stones used for riprap in prototype conditions are usually larger than 0.2 m.

The critical stone-related Froude number $\mathsf{F}_{s,c}$ for placed riprap is plotted as a function of slope in Figure 2(b) using data reported by Larsen et al. (1986), Dornack (2001), Peirson et al. (2008), Lia et al. (2013) and Hiller et al. (2017). The direct comparison of Figure 2(a) with Figure 2(b)

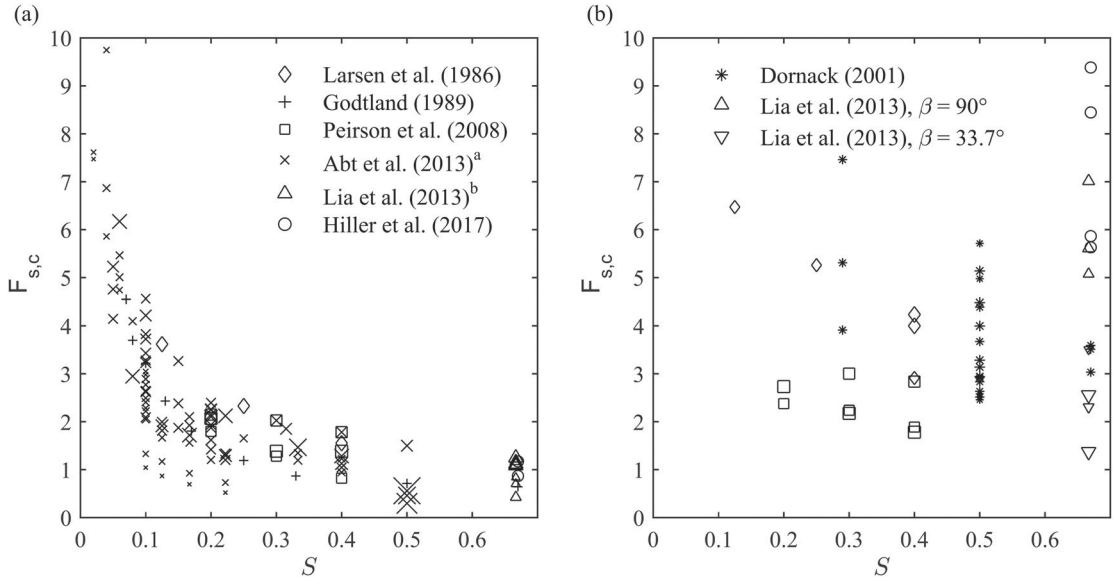

Figure 2. Existing data for the stability of dumped (a) and placed (b) riprap. The marker size is proportional to the used stone size (the marker size in the legend corresponds to $d = 0.1$ m). The legend for (a) applies also for (b). [a]The data from Abt et al. (2013) include data points of eight different studies. [b]Only data are presented from experiments with a locked dam toe.

reveals that $F_{s,c}$ scatters more for placed riprap than for dumped and that placed riprap is more stable, especially at steep slopes. Moreover, some studies found that the discharge capacity of the experimental facility was not large enough to induce failure of placed riprap (e.g. Sommer 1997; Lia et al. 2013; Hiller et al. 2017). For these studies, $F_{s,c}$ corresponded to $F_{s,c} > 3.3$ (Sommer 1997, with $0.25 \leq S \leq 0.5$ and $q_{max} = 0.5\,m^2s^{-1}$), $F_{s,c} > 3.1$ (Lia et al. 2013, with $S = 0.67$ and $q_{max} = 0.19\,m^2s^{-1}$) and $F_{s,c} > 11.5$ (Hiller et al. 2017, with $S = 0.67$ and $q_{max} = 0.49\,m^2s^{-1}$). Few design relationships have been developed specifically for placed riprap, as for example, by Knauss (1979), Sommer (1997) and Dornack (2001). These approaches were evaluated in Hiller et al. (2017) and are not discussed here.

A possible explanation for the variability of $F_{s,c}$ in Figure 2(b) is the difference in packing factors, which varied from $P_c = 0.53$ (Hiller et al. 2017) to $P_c = 0.65$ (Larsen et al. 1986), $P_c = 0.80$ (Dornack 2001) and $P_c = 0.94$ (Peirson et al. 2008). The different P_c values may be related to the shape of the stones used, in addition to the quality of the packing. The ratio between the longest and intermediate axes of the stones used in Hiller et al. (2017) was $a/b_s = 2.0$, and the stones were more oblong than in Dornack (2001), $1.4 < a/b_s < 1.8$, or Larsen et al. (1986), $a/d_s = 1.6$ (d_s was used instead of b_s due to missing information for b and c). No specific information about the stone shape was found for Peirson et al. (2008). Oblong stones placed with their a-axis towards the slope can be denser packed than stones having the same volume and a more cubical form, resulting in lower P_c values (Lindford and Saunders 1967). Moreover, Lia et al. (2013) found that denser arrangement of the riprap stones resulted in higher stability when varying the inclination angle β between the slope and the longest axes of the riprap stones (see Figure 1). They reported the highest stability for $\beta = 90°$, i.e. stones placed with their longest axes perpendicular to the slope. However, there was not sufficient information available in their study to determine P_c for a quantitative comparison with the aforementioned studies.

Studies with prototype-scale riprap are rare, but results from two previous field tests have recently been reported by Lia et al. (2013) and Hiller and Lia (2015). Lia et al. (2013) investigated the stability of placed riprap at a field site with prototype stones of $d_{50} = 0.65$ m (d_{50} is the stone size where 50% of the grains are finer by mass). Based on three tests, they concluded that the riprap stability increased with increasing inclination angle β. The test with $\beta = 71°$ (the target was $\beta = 90°$, but could not be achieved during construction) withstood the maximum available discharge per unit width of $q = 8.3\,m^2s^{-1}$, indicating $F_{s,c} > 5.1$. A comparative test with dumped riprap failed at $q_c = 2.1\,m^2s^{-1}$ ($F_{s,c} = 1.3$). Hiller and Lia (2015) used the same facility but a reduced stone size ($d_{50} = 0.54$ m) to achieve riprap failure with the available discharge. The placed riprap consequently failed at $q_c = 6.2\,m^2s^{-1}$ ($F_{s,c} = 5.1$) and $q_c = 2.0\,m^2s^{-1}$ ($F_{s,c} = 1.6$). It is worth mentioning that the latter riprap failed due to an instability in the riprap foundation. The corresponding result should therefore not be used for further analyses in regard to failure through overtopping, but it shows how construction-related boundary conditions can affect riprap-stability.

The construction-related properties of riprap might depend on the size of the riprap stones. However, reported results for prototype-scale riprap and corresponding model tests to analyse their comparability were not found. The

present study provides such a comparison and presents a novel set of both prototype and laboratory data for riprap on steep slopes.

3. Experiments

The stability of both dumped and placed riprap was tested at a temporary field site in Sirdal in Southwestern Norway and in the hydraulic laboratory at the Norwegian University of Science and Technology (NTNU) in Trondheim. The field tests were carried out with riprap stones of a mean diameter $d_{50} = 0.37$ m (herein defined as prototype tests) and the model tests with stones characterised by $d_{50} = 0.057$ m. The ratio of the prototype to model diameter results in a geometrical scale of 1:6.5 and the flow in the laboratory tests was subsequently scaled by applying Froude's model law. For both the laboratory and field experiments, the critical discharge q_c per unit width was defined as the discharge where progressive erosion of the riprap stones occurred. Moreover, the discharge for which erosion of the first riprap stone was observed, but did not necessarily result in a complete failure of the riprap, was denoted q_s. The corresponding critical stone-related Froude numbers are denoted as $F_{s,c}$ and $F_{s,s}$, respectively.

3.1. Field tests

Only a limited number of field tests could be carried out due to the pre-defined time frame provided by the dam owner, the logistics and available resources. As a consequence, two tests were carried out with placed riprap (F15P1 and F15P2) and one with dumped riprap (F15D1) within a period of three weeks. The test dams of approximately 3 m height and 12 m top width (9.5 m bottom width) were built in the outlet channel of a tunnel spillway, as shown in Figure 3.

The trapezoidal dam profile had an adverse slope of $S = 0.5$ upstream of the horizontal crest and a downstream slope of $S = 0.67$. The length of the downstream riprap cover in flow direction was $L_s \approx 4.5$ m. Ideally, this length should be longer to allow for flow development, but the achievable length was limited due to local peculiarities. Table 1 summarises the boundary conditions for the test dams.

Angular stones with $d_{50} = 0.37$ m were used for the riprap. The d_{50} was derived from the grain size distribution (by mass) of the nominal diameter $d = (abc)^{1/3}$ (Bunte and Abt 2001) of the riprap stones located in the central area of the riprap. The d_{50} is based on the analysis of a sample of 153 stones for which a, b and c were

Table 1. Boundary conditions for the field tests in 2015 including the dam height h_d, the dam width B, the reservoir level H_r, the inclination angle β and the packing factor P_c. The size of the riprap stones was $d_{50} = 0.37$ m, the extension of the slope covered with riprap $L_s \approx 4.5$ m and the target inclination angle $\beta_{target} = 60°$.

Test	h_d (m)	B (m)	H_r (m a.s.l.)	β (°)	P_c (–)
F15P1	3.2	12.2	896.03	53	0.75
F15P2	3.0	11.9	896.67	55	0.64
F15D1	3.1	12.5	897.03	–	0.84

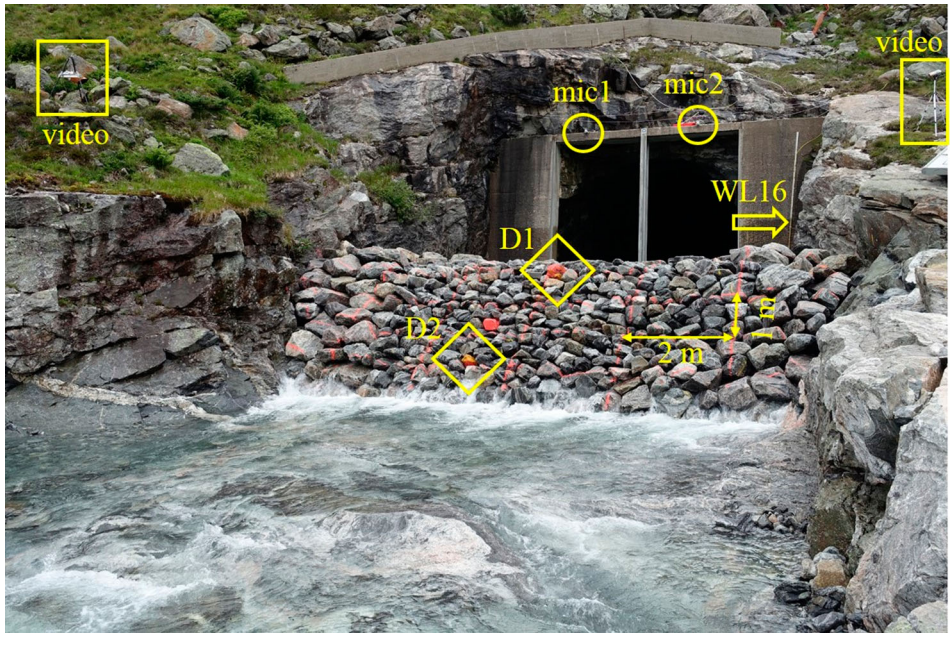

Figure 3. Test dam F15P2 between the two loadings. The highlighted measurement equipment indicates the positions of the video cameras, ultrasonic sensors mic1 and mic2, the pressure cell WL16 (the measuring point is behind the dam) and the equipped stones D1 and D2. (Photo: NTNU).

Table 2. Stone properties in terms of the average axes $\overline{a}, \overline{b}, \overline{c}$, the average stone diameter $\overline{d}$ and the d_{50}, coefficient of uniformity C_u, and density for the riprap stones ρ_s used in the field and for the model tests.

	$\overline{a}$ (m)	$\overline{b}$ (m)	$\overline{c}$ (m)	$\overline{d}$ (m)	d_{50} (m)	C_u	ρ_s (kg m^{-3})
F15	0.53	0.35	0.23	0.35	0.37	1.24	2750
Model	0.091	0.053	0.038	0.056	0.057	1.17	2710

measured manually using a folding rule (approximately 240 stones were used for the construction of the placed riprap). The riprap stones were slightly oblong ($a/b = 1.5$ in average) and the mass of the stones was estimated using $m = C_f \cdot \rho_s \cdot d^3$ (NVE 2012) with a shape factor $C_f = 0.48$. The grain size distribution of the stones can be characterised as uniform as the coefficient of uniformity $C_u = d_{60}/d_{10} = 1.24$ with $d_{\min} = 0.19$ m and $d_{\max} = 0.50$ m (see row F15 in Table 2).

The test dams were constructed with an excavator and the riprap covered the central part on the downstream slope and about 1 m of the crest (see Figure 3). The remaining part of the crest was secured with large stones (approximately 1.5–2 times the diameter of the stones used for the riprap) because the excavator was unable to reach this part to place the stones in an interlocking pattern. Furthermore, such large stones were used to lock the downstream end of the riprap, to prevent riprap failure along the abutments and to support the adverse upstream slope.

The construction of the test dams started with placing a row of large stones across the channel on the clean bedrock as dam toe. Afterwards, a permeable support fill consisting of angular stones with $d_{50} = 0.22$ m ($C_u = 2.3$) was constructed upstream of the initial stone row. Finally, the test dams were covered from down- to upstream with either placed or dumped riprap. The test dams were permeable and allowed a small percentage of the flow to pass through the dams as described and quantified later. Placed riprap for F15P1 and F15P2 was constructed by placing the stones one by one in an interlocking pattern and assuring that the longest axis of the stone (a-axis) was inclined towards the dam with a target angle $\beta = 60°$. The target angle differed intentionally from the most stable arrangement at $\beta = 90°$ to simulate a realistic inclination angle as typically observed in placed riprap on the downstream slopes of rockfill dams (Hiller 2016). The subsequent survey with an inclination meter (Leica DISTO ^{TM} X310; $\pm$ 0.2°) revealed angles of 53° and 55° for the two test dams, respectively, which were even lower than the target value. The packing factors corresponded to 0.75 and 0.64 (Table 1). The dumped riprap for test F15D1 was constructed by putting the stones on the slope with random orientation and without an interlocking pattern. Due to the steep slope, the stones could not be dumped and spread, but had to be put one by one by the excavator.

During overtopping, the water surface elevation at the tunnel outlet was monitored by two ultrasonic sensors (Microsonic™ mic + 340; $\pm$ 1%; referred to as 'mic1' and 'mic2') with a sampling frequency of 10 Hz. A pressure cell (Global Water™ WL16; $\pm$ 0.1%) installed at the side of the outlet in a zone of back flow measured the water depth with a sampling frequency of 0.1 Hz (Figure 3). Additional pressure sensors (Schlumberger Water Services™, Mini-Diver, DI501; $\pm$ 0.5 cm H_2O), usually used in groundwater wells, were installed along the dam to monitor the stage. Two additional pressure sensors were placed in riprap stones in drilled holes and secured with a bolted steal band. Sensor 'D1' was installed in a stone at the transition between the dam crest and the slope and 'D2' in a stone close to the dam toe (see Figure 3) to monitor the water level over the downstream slope. These two stones equipped with sensors were coloured to ease their recovery after riprap failure. Additional three pressure sensors were mounted in the rock under the test dams, and one sensor was installed approximately 2 m downstream of the dam (labelled with 'U1' to 'U4' from up- to downstream, not visible in Figure 3 because they are under the dam). The positions of the ultrasonic sensors, the pressure cell and sensors were measured with a handhold Leica™ GPS1200 (see Table A1 in the Appendix for the coordinates). The readings of the aforementioned sensors were used to determine the elevation of the water surface and averaged over 60 s. For each individual sensor, the reference level for the water depth corresponded to the measured water surface elevation at $F_s = 0.6$ ($q = 0.4\,m^2s^{-1}$) to compensate for some minor irregularities in dam construction (see dam height and width in Table 1) and the uneven surface of the dam due to the riprap stones. For this discharge, the riprap stones were just submerged (i.e. the water depth extracted from data corresponded approximately to the difference of the water surface elevation to the top of the riprap stones), and this definition enabled the calculation of the relative submergence $\Delta h_i/d_{50}$ for each sensor (the index i denotes the sensor; the reference level is sensor specific). All tests were monitored with three video cameras. A raster was sprayed on the test dams to facilitate visual monitoring and to determine the packing factor P_c.

Water was discharged from the reservoir by operating an outlet gate within the tunnel (2 m wide and 3 m high; not visible in Figure 3). The discharge was determined using the calibration curve of the gate, which was known from previous scale model tests (Vassdrags- og havnelaboratoriet 1973). The water level in the reservoir varied between the tests (see Table 1) which affected the discharge in the experiments for identical gate positions (differences of $< 1\%$ between corresponding gate openings for F15P1 and F15P2).

The placed riprap in F15P1 and F15P2 were loaded in a first step by opening the gate 0.4 m and releasing a discharge per unit width of $q = 1.6\,m^2s^{-1}$ for 60 min.

Following this initial loading period, the discharge was stopped to inspect the riprap for potential displacements or damage. Thereafter, $q = 0.4\,\mathrm{m^2s^{-1}}$ was released until the stage upstream of the dam stabilised, to estimate the percentage of flow passing through the permeable test dam, followed by 15 min of $q = 1.6\,\mathrm{m^2s^{-1}}$. Afterwards, the discharge was stepwise increased in 5-min intervals until the riprap failed. The increase in discharge was achieved by opening the gate additional 0.1 m resulting in increments of $\Delta q \approx 0.4\,\mathrm{m^2s^{-1}}$. The time interval was kept as short as possible to minimise the loss of water from the reservoir. Almost one million $\mathrm{m^3}$ of water was used for the three field tests and the water could consequently not be utilised for power production. The dumped riprap in test F15D1 was expected to fail at a significantly lower discharge than the placed riprap in the previous tests and loading started with $q = 0.2\,\mathrm{m^2s^{-1}}$. This discharge was applied until the stage remained stable to check the percentage of flow conveyed through the test dam. In the next step, the dam was overtopped for 30 min with $q = 0.4\,\mathrm{m^2s^{-1}}$. The riprap failed while increasing the discharge to $0.8\,\mathrm{m^2s^{-1}}$.

3.2. *Physical model tests*

Model tests were carried out with scaled discharges from the field tests to investigate the comparability of scale model tests with the prototype situation. A total of five model tests were carried out, four with placed riprap (P05–P08) and one with dumped, D02. In these tests, the discharge per unit width was scaled with $1{:}6.5^{1.5}$ and the time with $1{:}6.5^{0.5}$ according to Froude's model law using the geometrical scale defined above. The experimental setup, described in detail in Hiller et al. (2017), was built in a 1.00 m wide flume and consisted of an inclined chute with a horizontal crest (Figure 4), which were covered with a 0.1 m thick filter layer of angular stones with $d_{50} = 0.025$ m and $C_u = 1.50$. The chute and the adjacent 0.15 m of the crest were covered with riprap stones. The remaining part of the crest was secured with larger stones, similar to the field setup. Angular stones with $d_{50} = 0.057$ m and $C_u = 1.17$ were used for the riprap. These values were derived by weighing 500 stones and measuring their *a*, *b* and *c*-axis with a calliper (Table 2). Placed riprap was constructed by manually setting the stones one by one in an interlocking pattern with $\beta = 60°$. For the test with dumped riprap, the riprap stones were put one by one with random orientation and without interlocking pattern.

The packing factors and L_s are summarised in Table 3 together with the critical discharges for the erosion of the first stone q_s and riprap failure q_c. The placed riprap in tests P05, P06 and P07 did not fail when q was increased to the maximum possible discharge in the flume ($q_{max} = 0.49\,\mathrm{m^2s^{-1}}$ corresponding to $8.1\,\mathrm{m^2s^{-1}}$ in prototype scale). For these three tests, riprap failure was finally initiated by manually removing stones during overtopping. The test P08 was specifically designed to achieve riprap failure by extending the riprap length to $L_s = 1.8$ m as, for this riprap length, failure could be achieved with $q_c < 0.49\,\mathrm{m^2s^{-1}}$ in previous tests (Hiller et al. 2017).

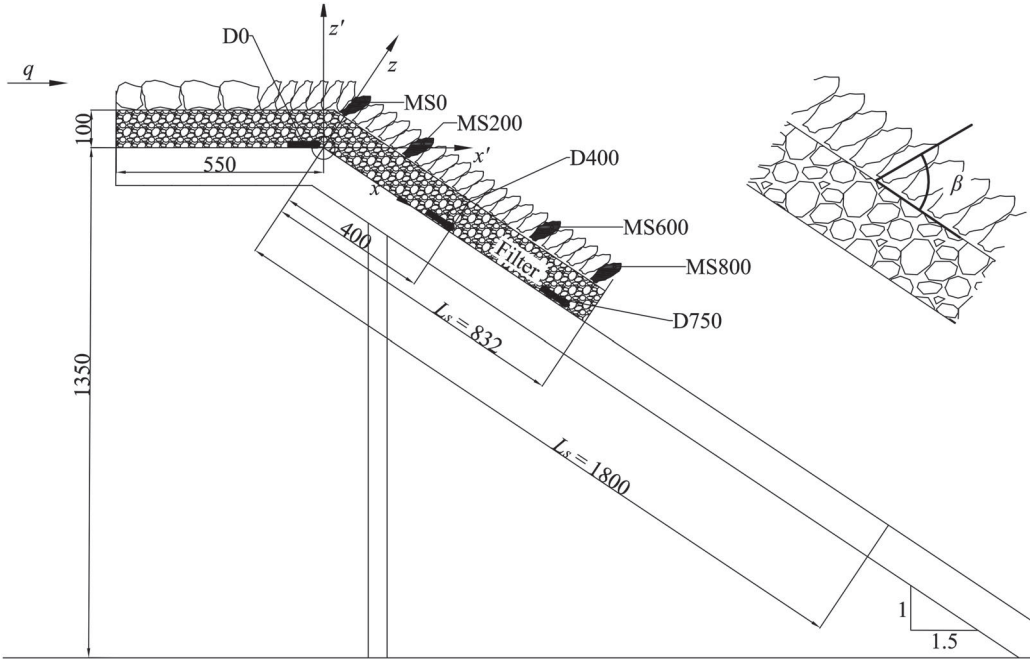

Figure 4. Setup for the scaled model tests with placed riprap P06 and P07. The chute was impervious and was overtopped with discharge from the left to the right. The marked stones 'MSxx' as well as the position of the pressure cells Diver 'Dxx' are marked. In the upper right corner, there is an enlarged part of the filter and the placed riprap stones to define the inclination angle β. All measures in mm.

Table 3. Experimental boundary conditions for the model tests including chute length covered with riprap L_s, packing factor P_c and the discharges per unit width q_s and q_c corresponding to erosion of the first stone and bulk erosion of the riprap, respectively.

Test	L_s (m)	P_c (–)	q_s (m^2s^{-1})	q_c (m^2s^{-1})	Δx_{init} (m)	Δx_{load} (m)
P05	1.0	0.48	<0.49	>0.49	0.000	0.006
P06	0.8	0.50	0.36	>0.49	0.002	0.010
P07	0.8	0.56	>0.49	>0.49	0.002	0.019
P08	1.8	0.55	0.19	0.24	0.038	–
D02	0.8	0.83	0.05	0.05	–	–

Notes: Δx_{init} and Δx_{load} denote the displacement in flow direction after the initial loading and up to q_{max}, respectively. All model tests were carried out with a stone size $d_{50} = 0.057$ m and a target stone inclination $\beta_{target} = 60°$.

As mentioned in Section 2, stone displacements can be crucial for the stability of placed riprap on steep slopes. In order to investigate the displacements in the flow direction, Δx, in the laboratory tests, the positions of four riprap stones were determined in P05–P07 with a laser displacement meter attached to traverse system. The stones were located in the middle of the flume at $x \approx 0.0$, 0.2, 0.6, 0.8 m (x indicates the distance in the flow direction from the edge between the horizontal crest and the slope, see Figure 4). Two additional stones were monitored in the test P08 due to the increased chute length. In this test, the stones were located at $x \approx 0.0$, 0.2, 0.6, 1.0, 1.4, 1.8 m. The measured maximum displacements, reported in Table 3, were always detected at the transition from the crest to the chute ($x \approx 0.0$ m). Note that in Table 3 Δx_{init} denotes the displacement after the initial loading and Δx_{load} after reaching q_{max}, but before manual interference.

The upstream water level was monitored 1.6 m upstream of the crest with an ultrasonic sensor of the same type as in the field. In order to monitor the water elevation over the riprap, pressure sensors (Schlumberger Water Services, Mini-Diver™, DI501; ±0.5 cm H_2O) were mounted along the centreline under the filter at $x \approx 0.00$, 0.40, 0.75 m for tests P06, P07 and D02, and $x \approx -0.2$, 0.2, 0.6, 1.0, 1.4 m for test P08 (see Figure 4; the sensor at $x \approx 0.2$ m turned out to be punctured and its data could not be used). No pressure sensors were installed for test P05, which was therefore excluded from the subsequent data analysis. The sampling frequency was 0.1 Hz for P06, 0.2 Hz for P07 and 1 Hz for P08 and D02. The sampling frequencies were adjusted according to the available memory of the pressure sensors and the assumed duration of the experiment. For the analysis below, the sensor data were averaged over 24 s corresponding to averaging over 60 s in the prototype. As for the prototype tests, the relative submergence $\Delta h_i/d_{50}$ was calculated using the stage at $F_s = 0.6$ as a reference for each sensor. The discharge to the flume was controlled by valves and delivered by two pipes equipped with discharge meters (Siemens Sitrans™ Mag5000; ±0.5%). All tests were monitored with two video cameras, one mounted in the flume facing the chute covered with riprap and the other facing the profile through the flume window.

4. Results and discussion

Table 4 summarises the packing factors and stone-related Froude numbers $F_{s,s}$ and $F_{s,c}$. The corresponding results will be presented and discussed below in regard to the riprap types.

4.1. *Dumped riprap*

The dumped riprap in the field test F15D1 failed during the increase of the discharge from 0.4 to 0.8 m^2s^{-1} (i.e. $0.6 < F_{s,c} < 1.2$) and the corresponding model test D02 failed at $F_{s,c} = 1.2$ ($q_c = 0.05\ m^2s^{-1}$). The packing factors in the field and model tests agreed well with $P_c = 0.84$ and $P_c = 0.83$, respectively, and $F_{s,c}$ was in the same range as the majority of the data points in Figure 2(a).

The flow in the prototype test during the lowest discharge step of $q = 0.2\ m^2s^{-1}$ ($F_s = 0.3$) is visualised in Figure 5(a). For this discharge, the main flow was conveyed through the permeable dam and the riprap was partly overtopped in the lower half of the test dam. This flow pattern can be associated with the dam-setup as the flow through the permeable dam body resulted in an increasing water level along the riprap. In the lower part, the flow pattern can be characterised as cascading over the riprap stones similar to nappe flow on stepped spillways. Despite this pattern, it can be reasonably assumed that the flow through the test dam was $q \leq 0.2\ m^2s^{-1}$. The cascading flow pattern prevailed also during the increased discharge of $q = 0.4\ m^2s^{-1}$ ($F_s = 0.6$; see Figure 5(b)). There were no visible differences in the flow pattern compared to the corresponding discharge over placed riprap (Figure 6(a)). The dumped riprap failed during a further

Table 4. Results of the field and model test in terms of the packing factor P_c and the stone-related Froude number for the erosion of the first stones $F_{s,s}$ as well as for riprap failure $F_{s,c}$.

Test	P_c (–)	$F_{s,s}$ (–)	$F_{s,c}$ (–)
F15P1	0.75	6.4	8.7
F15P2	0.64	8.9	10.6–11.3
F15D1	0.84	0.6–1.2	0.6–1.2
P05	0.48	<11.5[a]	>11.5
P06	0.50	8.4	>11.5
P07	0.56	<11.5[a]	>11.5
P08	0.55	4.5	5.6
D02	0.83	1.2	1.2

[a]The erosion of the first stone was not observed and the given value corresponds to the F_s when the first missing stone was detected.

Figure 5. Picture frames of the test F15D1 with dumped riprap: (a) partly overtopped test dam with most of discharge as through flow $q = 0.2\,\mathrm{m^2s^{-1}}$ ($\mathsf{F}_s = 0.3$); (b) cascading flow at $q = 0.4\,\mathrm{m^2s^{-1}}$ ($\mathsf{F}_s = 0.6$). (Video: S. R. Skilnand).

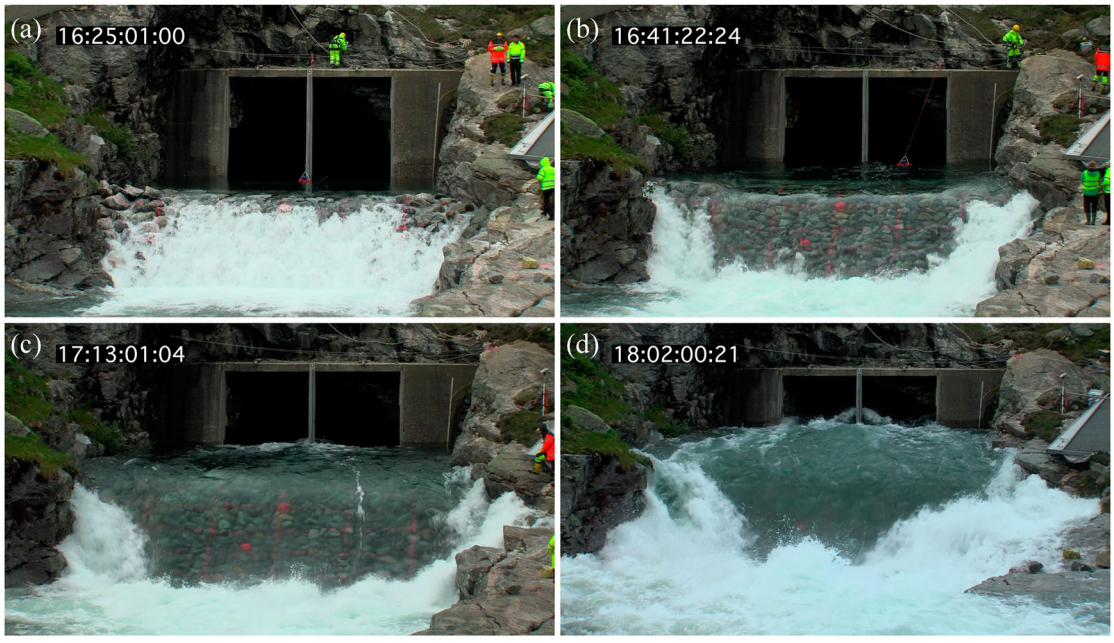

Figure 6. Picture series of F15P2: (a) nappe flow with $q = 0.5\,\mathrm{m^2s^{-1}}$ ($\mathsf{F}_s = 0.6$); (b) skimming flow with $q = 1.6\,\mathrm{m^2s^{-1}}$ ($\mathsf{F}_s = 2.3$); (c) skimming flow with still sound flow conditions upstream of the test dam at $q = 3.9\,\mathrm{m^2s^{-1}}$ ($\mathsf{F}_s = 5.5$); and (d) skimming flow in the centre part of the tests dam at $q = 7.5\,\mathrm{m^2s^{-1}}$ ($\mathsf{F}_s = 10.7$). The flow upstream of the test dam is uneven due to the inflow conditions and the high discharge of $Q = 90\,\mathrm{m^3s^{-1}}$. The coloured stone in the top containing D1 is missing because it was eroded at $q_s = 6.3\,\mathrm{m^2s^{-1}}$ ($\mathsf{F}_{s,s} = 8.9$). (Video: S. R. Skilnand).

increase in discharge as the central part of the riprap became unstable and slid down the supporting fill. Thereafter, the supporting fill was eroded as the protecting layer was missing. The flow pattern in the model tests corresponded to cascading flow as observed in the field. Moreover, the model crest was partly overtopped for $\mathsf{F}_s = 0.3$ ($q = 0.01\,\mathrm{m^2s^{-1}}$). Hence, it is reasonable to assume the portion of discharge corresponding to $\mathsf{F}_s = 0.3$ flowed through the test dams in the field and though the filter layer in the model tests, respectively.

4.2. Placed riprap

4.2.1. Stability and packing density

The placed riprap in the tests F15P1 and F15P2 failed at discharges corresponding to $\mathsf{F}_{s,c} = 8.6$ ($q_c = 6.1\,\mathrm{m^2s^{-1}}$) and $10.7 \leq \mathsf{F}_{s,c} \leq 11.3$ ($7.5\,\mathrm{m^2s^{-1}} \leq q_c \leq 8.0\,\mathrm{m^2s^{-1}}$; failed while increasing the discharge), respectively. In test F15P1, erosion of the first stone was observed at $\mathsf{F}_{s,s} = 6.4$ while in F15P2 four stones were eroded from the downstream edge of the crest at $\mathsf{F}_s = \mathsf{F}_{s,s} = 8.9$, among them the marked stone containing the sensor D1. Note that the flow through the permeable dam was included in the total discharge, but that it contributed less than 5% to $\mathsf{F}_{s,s}$ or $\mathsf{F}_{s,c}$.

The model tests P05, P06 and P07 withstood the maximum possible discharge $q_{max} = 0.49\,\mathrm{m^2s^{-1}}$, corresponding to $\mathsf{F}_s = 11.5$. The discharge could not be further increased as otherwise the inflow tank would have been overtopped. Therefore, discharges close to q_{max} were applied for a longer time period of up to 12 h. As this extended exposure of the riprap to overtopping did not result in failure, riprap failure was finally initiated by

manually removing stones during overtopping. Compared to the tests with shorter riprap length (P05–P07), the placed riprap in P08 with $L_s = 1.8$ m failed at $\mathsf{F}_{s,c} = 5.6$ ($q_c = 0.24\,m^2s^{-1}$) which may be attributed to the influence of displacements (see Hiller et al. 2017).

The reason for the observed differences in $\mathsf{F}_{s,c}$ for the field and laboratory tests may partly be associated with the packing of the riprap. In fact, the placed riprap in the field tests was looser packed and were characterised by significantly higher P_c values than the model tests (see Table 4). Constructing the riprap, it was challenging to keep the variation in P_c small as this parameter cannot be determined before finishing the riprap structure. As indicated by the numbering of the experiments, the placed riprap in the tests P05 and P06 were not the first riprap that were built in the laboratory (see Hiller et al. 2017 for a detailed overview on the laboratory experiments) and the low P_c values for these tests reflect that the experimentalists became more experienced in constructing the placed riprap. To counteract this tendency, the riprap stones in the subsequent tests P07 and P08 were randomly picked and placed in an interlocking pattern without further optimisation (keeping in mind the required inclination angle), resulting in increased P_c values for the respective tests. The different P_c values between the model ($P_c = 0.52$ on average) and the field tests ($P_c = 0.70$ on average) indicate laboratory effects in the placement, because the human dexterity allows denser packing compared to machine placement (Pardo et al. 2014). Moreover, differences in P_c can also result from the stone shape as the field-stones were slightly more cubical than the model-stones, apparent by the ratios $a/b_s = 1.8$ and $a/b_s = 2.0$, respectively.

4.2.2. *Flow pattern*

The visually observed flow patterns in the field and the model are first described and then compared with each other using exemplarily F15P2 in Figure 6 and P08 in Figure 7. A video of F15P2 is available in the supplementary material.

The flow pattern for the lowest field discharge resembled a nappe flow over the entire downstream slope (Figure 6(a)). When the discharge was increased, the flow became aerated and was, for $\mathsf{F}_s > 2.3$ ($q > 1.6\,m^2s^{-1}$), similar to a non-aerated skimming flow (Figure 6(b)). The flow along the abutments was affected by the uneven surface of the channel and the larger stones, resulting in boundary effects visible as white water (Figure 6(b–d)). Despite these boundary effects, the flow pattern in the centre of the test dams was still comparable to the corresponding pattern in the model tests shown in Figure 7. The marked stones were visible without difficulties up to $\mathsf{F}_s = 5.5$ ($q = 3.9\,m^2s^{-1}$, Figure 6(c)) and the water surface upstream of the dam was nearly flat and not much disturbed by the pillar in the tunnel opening. Upon a further increase of the discharge, the flow became more and more affected by the pillar causing a standing wave and an uneven water surface upstream of the test dams (Figure 6(d)). The hydraulic jump downstream of the test dams was not observed to affect the riprap stability.

In the model tests, the flow pattern in the upstream part in test P08 (Figure 7) corresponded the observed flow pattern in P05, P06 and P07, which were carried out with shorter L_s (indicated in the figure by the drawn horizontal line). Nappe flow occurred for $\mathsf{F}_s = 0.7$ ($q = 0.03\,m^2s^{-1}$, Figure 7(a)) which changed to skimming

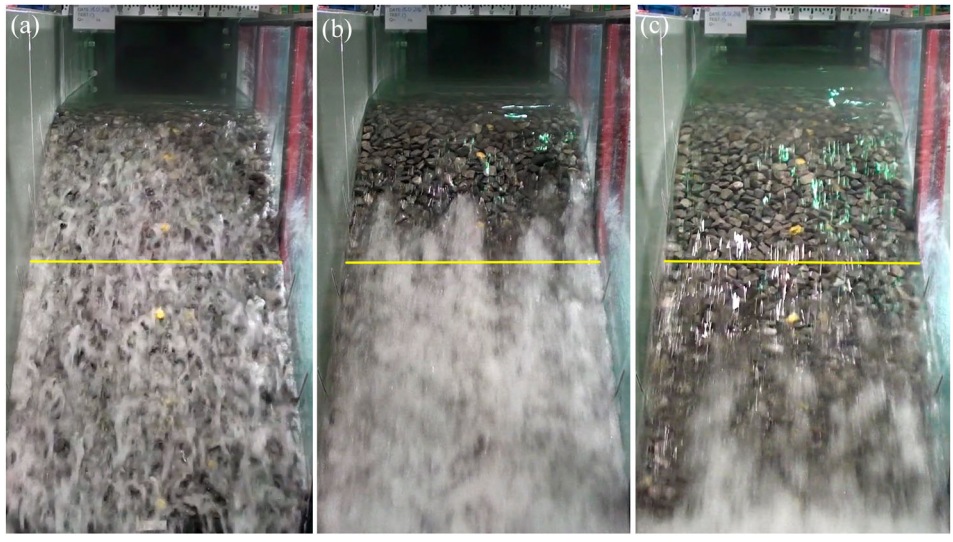

Figure 7. Video frames of P08. The yellow line at $x = 0.8$ m indicates the downstream end of the riprap in P06 and P07 and the corresponding field tests. (a) nappe flow over the whole slope at $q = 0.03\,m^2s^{-1}$ ($\mathsf{F}_s = 0.7$); (b) skimming flow without aeration in the upper third of the slope and aerated further downstream with $q = 0.10\,m^2s^{-1}$ ($\mathsf{F}_s = 2.4$); (c) skimming flow with partial aeration in the downstream third of the slope just before riprap failure at $q = q_c = 0.24\,m^2s^{-1}$ ($\mathsf{F}_s = \mathsf{F}_{s,c} = 5.6$). (Video NTNU).

flow when increasing the discharge. Self-aeration started around $x = 0.8$ m (corresponding to the dam toe in the field tests or the lower end of the riprap in the laboratory tests P05–P07) for $F_s = 2.4$ ($q = 0.10\,m^2s^{-1}$, Figure 7(b)). The point of aeration moved further downstream with increasing discharge, as was observed in the field where aeration could no longer be observed for $F_s > 2.3$ ($q > 1.6\,m^2s^{-1}$, Figure 6(b)). Accordingly, the aeration started downstream of the drawn line in Figure 7(c), indicating the scaled L_s of the prototype tests. The figure shows P08 just before riprap failure at $F_s = 5.6$ ($q = 0.24\,m^2s^{-1}$).

4.2.3. *Pressure measurements and water levels*

The relative submergence $\Delta h_i/d_{50}$ upstream of the riprap corresponds to the relative overtopping depth over the test dams in the field and model and is presented in Figure 8 as a function of F_s. The figure shows two data series for each field test representing the two different sensor types 'mic' (average of 'mic1' and 'mic2') and 'WL16'. The deviation between the two sensor readings can be attributed to the different locations of the sensors (see Figures 3 and 6). The comparison of the field values $\Delta h_{mic}/d_{50}$ with the data from the model tests shows good agreement for $F_s < 6$, before the two series deviate for higher F_s. The deviation can be attributed to the undulating water surface in the field for $F_s > 6$ (see Figure 6(c,d)). Furthermore, changes in the dam crest due to stone displacements might have an effect on the overtopping characteristics in the field and hence the relation between the unit discharge and the overtopping depth. This assumption is supported for F15P1 by the observation of stone erosion from the crest at $F_{s,s} = 6.4$. The shape of the curves for the model tests P06, P07 and P08 in Figure 8 is regular and no deviation is visible around $F_s = 6$ indicating that the discharge coefficient of the crest did not change. This is supported by the observation that only small stone displacements ($\Delta x_{load} < 0.020$ m, Table 3) developed close to the transition between the crest and the slope in the model tests P05–P07. Note that this does not contradict the statement above that displacements can be crucial for the stability of placed riprap on steep slopes. The displacements did not exceed the critical size of one stone length (Hiller et al. 2017), implying that the placed riprap was still stable, and reflected by the fact that the riprap in P05–P07 did not fail.

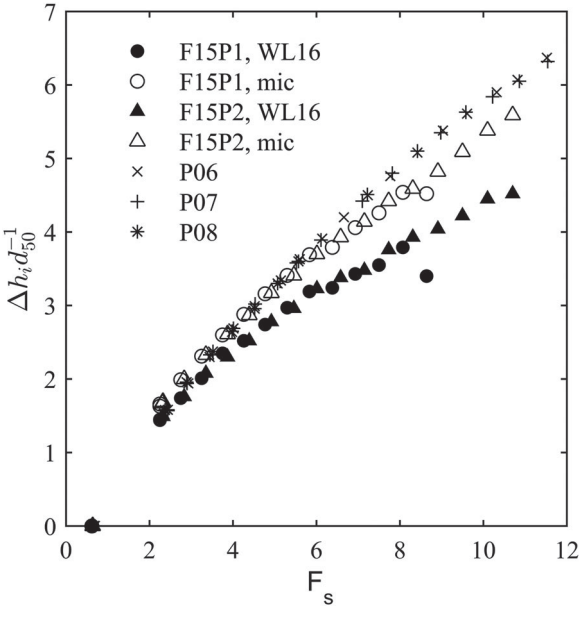

Figure 8. Relative submergence $\Delta h_i/d_{50}$ as a function of the stone-related Froude number for the field and model tests.

The relative submergence $\Delta h_i/d_{50}$ measured by the pressure sensors is plotted as a function of F_s in Figures 9 and 10 for the field and model tests, respectively. The data for the field sensors D1 and D2 in Figure 9(a) agree well with the observation of the flow pattern and the relative overtopping depth for $\Delta h_{mic}/d_{50}$ as described above. The gradient for $\Delta h_{D1}/d_{50}$ for F15P1 and F15P2 changes at $F_s = 5.8$, when the undulating water level due to the pillar became more important, and when a change in the discharge coefficient of the crest due to the erosion of several stones from the crest might have occurred at $F_s = F_{s,s} = 6.4$. It is worth mentioning that the sensors mounted inside riprap stones could not be placed exactly at the same location in F15P1 and F15P2. The different sensor locations provide an explanation for the offset between $\Delta h_i/d_{50}$ for F15P1 and F15P2. The series $\Delta h_{D1}/d_{50}$ for F15P2 is limited to $F_s \leq 8.3$ as the stone containing D1 was eroded at $F_s = 8.3$.

Figure 9(b) shows the data of the pressure sensors which were located under the tests dams and which were not moved between the field tests. The increasing flow irregularities due to the high discharge and the consequent destabilisation of the riprap are reflected by the increasing scatter for $F_s > 6.4$ in the F15P1 data series. The difference in the gradient of the data series $\Delta h_{U2}/d_{50}$ and $\Delta h_{U3}/d_{50}$ for both field tests indicates that the flow was still under acceleration over the riprap. The sensor U4 was mounted 2 m downstream of the test dam in F15P1 and hence $\Delta h_{U4}/d_{50}$ deviates from the other data series. During riprap failure in F15P1, the sensor was damaged and not replaced for the subsequent tests.

Figure 10 presents the data of the pressure sensors recorded during the model tests. The pressure sensors were placed at different locations compared to the field tests and a direct comparison with the field data is therefore hampered. The data series in Figure 10(a) for the model tests P06 and P07, which were carried out with a chute length corresponding to the scaled test dams in the field, have different gradients affirming non-uniform flow over the riprap. The larger deviations for $\Delta h_{D0}/d_{50}$ between P06 and P07 can be attributed to the close position of the sensor to transition from sub- to supercritical flow and the corresponding rapid change in h, meaning that small differences in the riprap constructions can affect the recordings at this

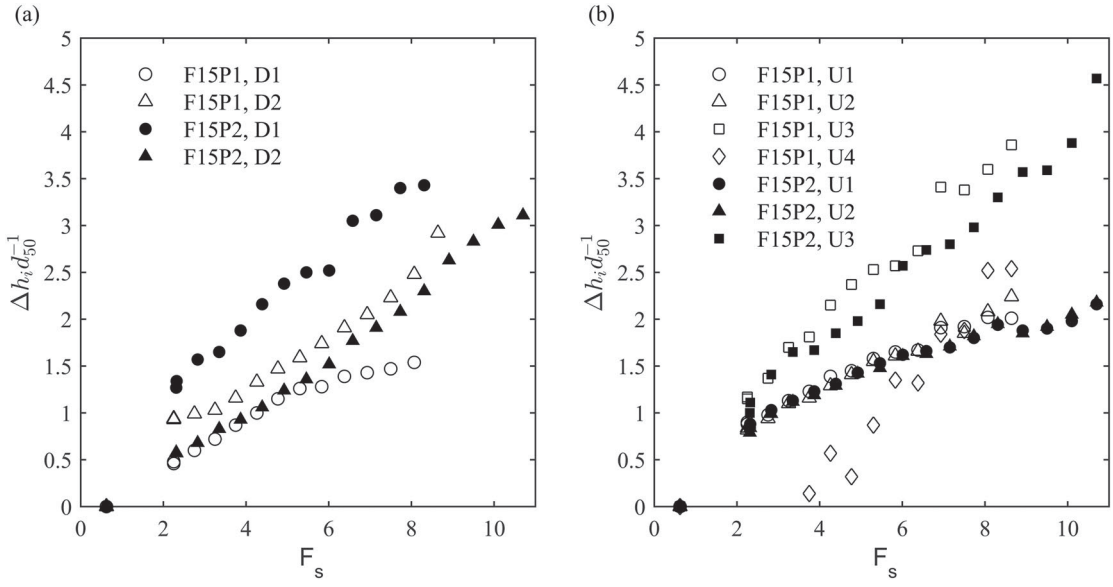

Figure 9. Relative submergence as a function of F_s for the data of the pressure cells during the field tests: (a) Data of the sensors D1 and D2 placed in riprap stones. (b) Data of the sensors placed in the bottom of the channel, U1 to U3 under the test dams and U4 approximately 2 m downstream (damaged under F15P1 and not replaced for the remaining tests).

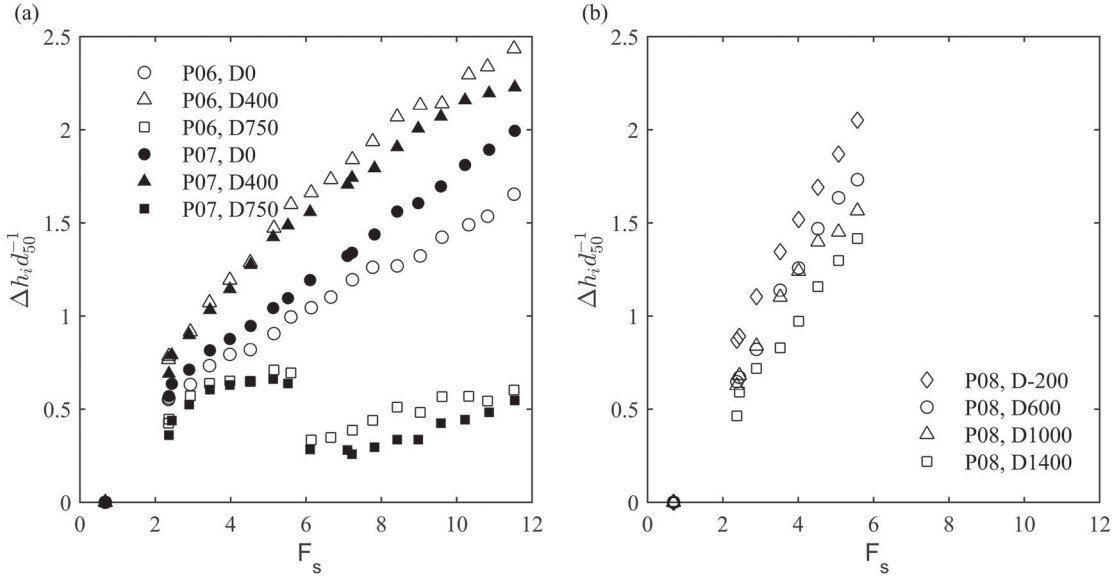

Figure 10. Relative submergence as a function of F_s for the data recorded by the pressure cells in the model tests. The number in the label indicates the distance in mm to the edge between the crest and the slope in flow direction. Data of P06 and P07 in (a) and of P08 in (b).

particular location. A significant decrease in $\Delta h_{D750}/d_{50}$ for $5.6 < F_s < 6.1$ coincides with the observation that the point of aeration passed the downstream end of the riprap. The data of P08 are presented separately in Figure 10(b) because P08 was carried out with increased chute length of 1.8 m and the pressure cells were mounted at different locations than in P06 and P07. The data series for $\Delta h_{D600}/d_{50}$, $\Delta h_{D1000}/d_{50}$ and $\Delta h_{D1400}/d_{50}$ in P08 have a similar gradient.

4.3. Comparison between dumped and placed riprap

The critical stone-related Froude numbers in the present study were $F_{s,c} \leq 1.2$ for dumped riprap and $F_{s,c} \geq 5.6$ for placed riprap (Table 4). The values for dumped riprap are in the same range as reported in the literature (see Figure 2(a)) whereas $F_{s,c}$ for placed riprap are generally larger than the values reported by Larsen et al. (1986), Dornack (2001) and Peirson et al. (2008) (see Figure 2(b)). However, these studies were carried out on gentler slopes,

except for the three experiments of Dornack (2001) with $S = 0.67$. The field tests with placed riprap and a comparable stone inclination β reported by Lia et al. (2013) and Hiller and Lia (2015) had similar $F_{s,c}$ than in the present study. The stability of placed riprap in terms of $F_{s,c}$ is on average nine times higher than for dumped riprap (based on the data in Table 4, using $F_{s,c} = 11.5$ for P05–P07) and is hence larger than the stability gain between dumped and placed riprap in the study by Larsen et al. (1986) or Peirson et al. (2008). The stability gain is also higher than the gain reported in Hiller et al. (2017). However, Hiller et al. (2017) focused solely on results from the laboratory study and did not include the results of the field tests, excluding also the results of P05–P07. Possible reasons for the different stability gain compared to Larsen et al. (1986) and Peirson et al. (2008) are the different packing factors and boundary conditions in terms of the chute length.

The packing factors for dumped riprap were nearly identical in the prototype and the model scale. On the other hand, the placed riprap in the field tests was looser packed (i.e. higher P_c values) than in the model tests. This observation indicates laboratory effects, which are present for placed, but not for dumped riprap.

The scope of this paper is the comparability of large-scale and model-scale riprap tests and a generalisation of the results in terms of a riprap sizing formula was abandoned due to the limited number of data points with similar packing factors. However, the packing factor can be used as an indicator for the quality of placed riprap. A detailed description of placed riprap in terms of used stone size and shape, placement pattern and packing density is crucial to allow comparison with different studies.

5. Conclusions

Unique field tests were carried out with large-scale riprap and compared with corresponding model tests in the scale of 1:6.5. The comparability between the model and laboratory tests was investigated in terms of stability, packing density, flow pattern and overtopping depth. Measurements of the upstream water level and along the riprap helped to detect flow changes, which were a consequence of changes in the riprap. The study showed good agreement for the dumped riprap tests between the field and the model tests in terms of the critical stone-related Froude number, packing factors and flow pattern. Placed riprap showed good comparability in the visually observed flow pattern and the relative overtopping depth, but the stability in terms of the stone-related Froude number was higher in the model tests. The packing factor was lower in the model, indicating denser packing than in the field, and gives a possible explanation for the deviation in stability between the model and the field tests. The packing factor seems to be an adequate measure to describe the quality of placed riprap. However, it is challenging to control this construction-related parameter and laboratory effects in the packing factor should be considered and further evaluated.

Acknowledgements

We thank the Master students Fredrikke Kjosavik and Bastian Dost for their help in carrying out the physical model tests and field tests and the staff in the NTNU hydraulic laboratory for technical assistance. The collaboration and support by Sira-Kvina Power Company for access to the field site at dam Svartevatn and water supply are kindly acknowledged. The permissions to use the reports of Larsen et al. (1986) and Sommer (1997) by the Regierungspräsidium Karlsruhe and the Karlsruhe Institute of Technology are acknowledged. We thank also the editor and reviewers for their comments, which helped to improve this paper.

Funding

This work was supported by the Research Council of Norway [project number 235730]; Energy Norway under [project PlaF].

Supplemental data

Supplemental data for this article can be accessed at https://doi.org/10.1080/23249676.2018.1449675.

Notes on contributors

Priska H. Hiller holds an MSc in Civil Engineering from the Swiss Federal Institute of Technology ETH Zurich. She worked as a consultant in hydraulics and hydrology at Sweco Norway AS before she did her PhD at the Norwegian University of Science and Technology (NTNU) in Trondheim 2013–2017. She works currently at the Norwegian Water Resources and Energy Directorate and the Young Engineers Forum of the International Commission on Large Dams (ICOLD).

Leif Lia graduated from Norges tekniske høyskole (NTH) in 1993 and his PhD was completed in 1998 at NTNU. He worked for Grøner/Sweco Norway AS consulting company for 11 years, seven years as head of the Hydropower department and simultaneously nine years as assistant professor (20%) in Dam Safety at NTNU. Since 2009, he has been Professor in hydropower structures in the Department of Civil and Environmental Engineering at NTNU. He is currently Vice President of ICOLD in 2014–2017.

Jochen Aberle received his education in civil engineering from the University of Karlsruhe (TH), Germany, with a diploma in 1996 and the PhD title in 2000. After a two years postdoctoral stay at the National Institute of Water and Atmospheric Research (NIWA) in Christchurch NZ, he joined the Leichtweiss-Institute for Hydraulic Engineering and Water Resources (LWI) at the Technische Universität Braunschweig in 2003. In 2012, he became full Professor at NTNU in Trondheim. In 2017, he moved back to LWI as a full Professor, still holding a 20% position at NTNU.

ORCID

Priska H. Hiller http://orcid.org/0000-0002-7639-5358
Jochen Aberle http://orcid.org/0000-0002-5435-2832

References

Abt SR, Johnson TL. 1991. Riprap design for overtopping flow. J Hydraul Eng. 117:959–972.

Abt SR, Thornton CI, Scholl BA, Bender TR. 2013. Evaluation of overtopping riprap design relationships. J Am Water Resour Ass. 49:923–937.

Bung DB. 2013. Non-intrusive detection of air–water surface roughness in self-aerated chute flows. J Hydraul Res. 51:322–329.

Bunte K, Abt SR. 2001. Sampling surface and subsurface particle-size distributions in wadable gravel- and cobble-bed streams for analyses in sediment transport, hydraulics, and streambed monitoring. Fort Collins, CO (USA): USDA, Rocky Mountain Research Station. General Technical Report; RMRS-GTR-74.

Chanson H. 2015. Embankment overtopping protection systems. Acta Geotechnica. 10:305–318.

CIRIA, CUR, CETMEF. 2007. *The rock manual: The use of rock in hydraulic engineering*, 2nd ed. London: CIRIA.

Deutscher Verband für Wasserwirtschaft und Kulturbau [DVWK]. 1990. *Hydraulische Methoden zur Erfassung von Rauheiten* [Hydraulic methods to determine roughnesses]. Hamburg: Parey.

Dornack S. 2001. Überströmbare Dämme – Beitrag zur Bemessung von Deckwerken aus Bruchsteinen [Overtoppable dams – a contribution to the design of riprap] [dissertation]. Dresden (Germany): Technische Universität Dresden. German.

Godtland K. 1989. *Steinfyllingsdammer: dimensjonering av nedstrøms plastringsstein unntatt damfoten* [Rockfill dams: design of riprap stones on the downstream slope except the dam toe]. Trondheim: Norsk hydroteknisk laboratorium. (ISBN: 82-595-5892-0). Norwegian.

Harris MJ. 2015. Failure of dams due to overtopping – a historical prospective. In: Toledo MA, Morán R, Oñate E. Proceedings of the Dam Protections against Overtopping and Accidental Leakage – Proceedings of the 1st International Seminar on Dam Protections Against Overtopping and Accidental Leakage; 2014 Nov 24–26; Madrid: CRC Press/Balkema.

Hiller PH. 2016. *Kartlegging av plastring på nedstrøms skråning av fyllingsdammer*. Trondheim [Survey of placed riprap on the downstream slope of rockfill dams]. Trondheim: Norwegian University of Science and Technology. (ISBN-10: 978-827598-095-1). Norwegian.

Hiller PH, Aberle J, Lia L. 2017. Accumulating stone displacements as failure origin in placed riprap on steep slopes. J Hydraul Res. [Internet]. [Published online 2017 June 27]. doi:10.1080/00221686.2017.1323806.

Hiller PH, Lia L. 2015. Practical challenges and experience from large-scale overtopping tests with placed riprap. In: In: Toledo MA, Morán R, Oñate E. Proceedings of the Dam Protections against Overtopping and Accidental Leakage - Proceedings of the 1st International Seminar on Dam Protections Against Overtopping and Accidental Leakage; 2014 Nov 24–26; Madrid: CRC Press/Balkema.

International Commission on Large Dams [ICOLD]. 1995. *Dam failures statistical analysis*. Paris: ICOLD.

Jafarnejad M, Franca MJ, Pfister M, Schleiss AJ. 2016. Time-based failure analysis of compressed riverbank riprap. J Hydraul Res. [Internet]. [published online 2016 Aug 23; cited 2016 Nov 30]; 12. doi:10.1080/00221686.2016.1212940.

Knauss J. 1979. Computation of maximum discharge at overflow rockfill dams (a comparison of different model test results). In: International Commission on Large Dams. 13th Congress on Large Dams; 1979; New Delhi.

Larsen P, Bernhart HH, Schenk E, Blinde A, Brauns J, Degen FP. 1986. Überströmbare Dämme, Hochwasserentlastung über Dammscharten [Overtoppable dams, spillways over dam notches] (unpublished report prepared for Regierungspräsidium Karlsruhe). Karlsruhe (Germany): Universität Karlsruhe. German.

Lia L, Vartdal EA, Skoglund M, Campos HE. 2013. Rip rap protection of downstream slopes of rock fill dams – a measure to increase safety in an unpredictable future climate. Paper presented at: 9th ICOLD European Club Symposium; Venice.

Linford A, Saunders DH. 1967. A hydraulic investigation of through and overflow rockfill dams. British Hydromechanics Research Association.

Løvoll A. 2006. Breach formation in rockfill dams – results from Norwegian field tests. In: International Commission on Large Dams. 22nd Congress on Large Dams; 2006 Jun; Barcelona.

Ministry of Petroleum and Energy [OED]. 2009. Forskrift om sikkerhet ved vassdragsanlegg (Damsikkerhetsforskriften) [Dam safety regulation]. OED. (FOR 2009-12-18-1600). Norwegian.

Mishra SK. 1998. Riprap design of overtopped embankments [dissertation]. Fort Collins (CO): Colorado State University.

Morán R, Toledo MA. 2011. Research into protection of rockfill dams from overtopping using rockfill downstream toes. Can J Civil Eng. 38:1314–1326.

Morris MW, Hassan MAAM, Vaskinn KA. 2007. Breach formation: field test and laboratory experiments. J Hydraul Res. 45:9–17.

Norwegian Water Resources and Energy Directorate [NVE]. 2012. *Veileder for Fyllingsdammer* [Guidelines for embankment dams]. Oslo: NVE. (guideline 4/2012). Norwegian.

Olivier H. 1967. Through and overflow rockfill dams – new design techniques: Institution of Civil Engineers. Paper no. 7012.

Pagliara S, Carnacina I, Roshni T. 2010. Self-Aeration and friction over rock chutes in uniform flow conditions. J Hydraul Eng. 136:959–964.

Pardo V, Herrera M, Molines J, Medina J. 2014. Placement test, porosity, and randomness of cube and cubipod armor layers. J Waterway Port Coast Ocean Eng. 140:04014017.

Peirson WL, Cameron S. 2006. Design of rock protection to prevent erosion by water flows down steep slopes. J Hydraul Eng. 132:1110–1114.

Peirson WL, Figlus J, Pells SE, Cox RJ. 2008. Placed rock as protection against erosion by flow down steep slopes. J Hydraul Eng. 134:1370–1375.

Robinson KM, Rice CE, Kadavy KC. 1998. Design of rock chutes. Trans Am Soc Agric Eng. 41:621–626.

Schmocker L, Höck E, Mayor P, Weitbrecht V. 2013. Hydraulic model study of the fuse plug spillway at Hagneck canal, Switzerland. J Hydraul Eng. 139:894–904.

Siebel R. 2007. Experimental investigations on the stability of riprap layers on overtoppable earthdams. Environ Fluid Mech. 7:455–467.

Sommer P. 1997. Überströmbare Deckwerke [Overtoppable erosion protections] (unpublished report). Karsruhe (Germany): Institut für Wasserbau und Kulturtechnik, Versuchsanstalt für Wasserbau, Universität Karlsruhe. German.

Toledo MÁ, Morán R, Oñate E, editors. 2015. *Dam protections against overtopping and accidental leakage*. London: CRC Press/Balkema.

Vassdrags-og havnelaboratoriet. 1973. Dam Svartevann, flomløp: Øvre tappeluke, kalibreringskurver [Dam Svartevann, spillway: upper releasing gate, calibration curves]. Trondheim (Norway): Vassdrags- og havnelaboratoriet ved Norges tekniske høgskole. Norwegian.

Appendix

Table over coordinates of the measuring equipment in 2015.

Table A1. Coordinates for the pressure cell WL16, microsonic sensors mic1 and mic2 and the pressure sensors ('U' indicating placement under the dam and 'D' on the dam, numbering from upstream to downstream). Coordinates given in Euref89 UTM32, height in NN1954.

	Item	*X* (m)	*Y* (m)	*Z* (m)
All tests	WL16	n/a	n/a	772.27
	mic1	6,556,225.31	329,769.55	777.94
	mic2	6,556,224.28	329,766.01	777.91
	U1	6,556,213.90	329,770.65	770.74
	U2	6,556,212.51	329,770.22	770.88
	U3	6,556,210.94	329,771.89	770.85
F15P1	Bottom left	6,556,211.23	329,776.05	771.38
	Bottom right	6,556,209.17	329,766.81	771.42
	Top right	6,556,211.94	329,764.89	773.88
	Top left	6,556,215.76	329,776.48	774.05
	D1	6,556,214.60	329,770.58	773.95
	D2	6,556,211.23	329,771.29	772.11
	U4	6,556,208.27	329,771.90	771.04
F15P2	Bottom left	6,556,211.80	329,776.04	771.24
	Bottom right	6,556,210.11	329,766.82	771.26
	Top right	6,556,212.76	329,764.62	773.85
	Top left	6,556,215.42	329,776.25	773.59
	D1	6,556,214.50	329,770.69	773.70
	D2	6,556,211.70	329,770.18	772.11
F15D	Bottom left	6,556,211.77	329,776.15	771.33
	Bottom right	6,556,210.09	329,766.83	771.24
	Top right	6,556,212.60	329,764.56	773.80
	Top left	6,556,215.52	329,776.70	773.84
	D1	6,556,213.85	329,770.51	773.57
	D2	6,556,211.46	329,771.84	771.68